Search for low-lying lattice QCD eigenstates in the Roper regime

Adrian L. Kiratidis,[*] Waseem Kamleh, Derek B. Leinweber, Zhan-Wei Liu, Finn M. Stokes, and Anthony W. Thomas

Special Research Centre for the Subatomic Structure of Matter, Department of Physics,
University of Adelaide, South Australia 5005, Australia

The positive-parity nucleon spectrum is explored in $2 + 1$ flavor lattice QCD in a search for new low-lying energy eigenstates near the energy regime of the Roper resonance. In addition to conventional three-quark operators, we consider novel, local five-quark meson-baryon type interpolating fields that hold the promise to reveal new eigenstates that may have been missed in previous analyses. Drawing on phenomenological insight, five-quark operators based on σN, πN and $a_0 N$ channels are constructed. Spectra are produced in a high-statistics analysis on the PACS-CS dynamical gauge-field configurations with $m_\pi = 411$ MeV via variational analyses of several operator combinations. Despite the introduction of qualitatively different interpolating fields, no new states are observed in the energy regime of the Roper resonance. This result provides further evidence that the low-lying finite-volume scattering states are not localized, and strengthens the interpretation of the Roper as a coupled-channel, dynamically-generated meson-baryon resonance.

I. INTRODUCTION

Since the inception of lattice QCD, significant effort has been invested in exploring hadronic spectra, both to shed light upon the nature and properties of various states, and to test the validity of the methodology itself. In particular, the community has shown notable interest in the positive-parity nucleon channel [1–6], where the first positive-parity $J^P = \frac{1}{2}^+$ excitation of the nucleon, known as the Roper resonance $N^*(1440)$, remains a puzzle.

In Nature, the Roper lies 95 MeV below the lowest-lying negative-parity resonant state, the $N^*(1535)$, whereas in constituent quark models (where it is associated with an $N = 2$ radial excitation of the nucleon) the order is reversed [7–9]. Speculation about the true nature of this state has been widespread, including the idea that the Roper can be understood with five-quark meson-baryon dynamics [10].

A critical challenge for lattice spectroscopy in this channel is to judiciously choose an appropriate operator basis to sufficiently span states of interest in the low-lying spectrum. This can be achieved in multiple ways. Recalling that any radial function can be expanded using a basis of different width Gaussians, $f(|\vec{r}|) = \sum_i c_i e^{-\varepsilon_i r^2}$, suggests the use of fermion sources with varying Gaussian smeared widths [11], which is one method to obtain a basis of operators possessing enhanced overlap with radial excitations.

The CSSM lattice collaboration was the first to demonstrate that the inclusion of Gaussian-smeared fermion sources of wide widths are critical in enabling the extraction of the lowest-lying positive-parity excitation in the nucleon channel [1,12]. It was later shown that the quark

probability distribution for this state is consistent with an $N = 2$ radial excitation [3,13].

Another method for selecting an appropriate operator basis is to include qualitatively different operators, by introducing interpolating fields with the same quantum numbers but different quark and/or Dirac structure. Here, it becomes instructive to briefly examine the contemporary work done in the negative-parity nucleon channel with its two low-lying resonances, the $N^*(1535)$ and $N^*(1650)$ [2,14–17].

In recent years the CSSM and Hadron Spectrum lattice collaborations have studied the low-lying negative-parity spectrum of the nucleon using various local three-quark operators [2,16–20] but were unable to extract a state consistent with the low-lying S-wave πN scattering threshold. Notably, at near physical quark masses this threshold lies below the lowest-lying negative-parity resonant state, making it an intuitive place to search for the presence of states consistent with scattering thresholds.

However, for states dominated by a two-particle scattering component, the probability of finding the second particle at the position of the first is proportional to $1/V$, where V is the spatial volume of the lattice. Therefore, the coupling of these scattering states to local operators is volume suppressed.

Naturally, one would expect five-quark operators to possess higher overlap with five-quark states, and as such the CSSM lattice collaboration introduced local five-quark πN-type operators [21]. These operators were constructed from a negative-parity pion piece together with a positive-parity nucleon piece. Consequently, the operators were expected to possess higher overlap with the S-wave πN scattering state and, indeed, a state consistent with this threshold was observed. However, the coupling was

---

[*]adrian.kiratidis@adelaide.edu.au

074507-1

relatively weak, and one can conclude that the S-wave πN scattering state is poorly localized and better treated with an approach in which the momenta of both the pion and the nucleon are projected to zero. These nonlocal operators are known to have excellent overlap with the scattering state [15].

Turning to the positive-parity channel, we are searching for new states that have poor overlap with conventional three-quark operators and therefore have been missed in analyses to date. Meson-baryon states having strong attraction, which can give rise to localization of the state [22], are expected to have good overlap with our local five-quark operators. The existence of such states would suggest an important role for molecular meson-baryon configurations [23] in the formation of the Roper resonance.

To obtain positive parity in a local meson-baryon interpolating field, the intrinsic parities of the meson and baryon must match, and there are two approaches one can consider. Because the lowest-lying five-quark scattering state is a πN *P*-wave state, previous attempts have considered the approach of local πN-type interpolators. As the ability to construct a relative *P*-wave πN does not exist in a local operator, this approach necessarily draws on an odd-parity excitation of the nucleon to form the quantum numbers of the Roper. As one might expect, this operator had negligible overlap with the *P*-wave πN scattering threshold which lies between the ground state and the first positive-parity excitation observed in lattice QCD at light quark masses. No state consistent with this threshold was observed in the five-quark analysis of Ref. [21].

Drawing on the success of the local πN-type operator in the negative parity sector, we consider the alternative approach of pairing an even-parity meson interpolator with the nucleon interpolator such that the ground state nucleon can participate in forming the positive-parity quantum numbers of the Roper resonance. In this analysis, we construct the local five-quark meson-baryon operators $a_0 N$ and σN, and investigate their impact on the positive-parity nucleon spectrum. We search for both new low-lying eigenstates in the finite volume of the lattice, and/or an alteration of the spectrum reported in previous analyses.

Following the outline of variational analysis techniques in Sec. II, we construct the new local five-quark operators in Sec. III, and outline the stochastic-noise methods employed to calculate the corresponding loop containing diagrams. Simulation details are discussed in Sec. IV and the results of the variational analyses are presented in Sec. V. A summary of our findings and their impact our understanding of the Roper resonance is presented in Sec. VI.

II. CORRELATION MATRIX TECHNIQUES

Correlation matrix based variational analyses [24,25] are now well-established as a framework within which hadron spectra can be produced [26]. The methodology begins via the judicious selection of a suitably large basis of N operators, such that the states of interest within the spectrum are contained within the span. An $N \times N$ matrix of cross correlation functions,

$$\mathcal{G}_{ij}(\vec{p}, t) = \sum_{\vec{x}} e^{-i\vec{p}\cdot\vec{x}} \langle \Omega | \chi_i(\vec{x}, t) \bar{\chi}_j(\vec{0}, t_{\text{src}}) | \Omega \rangle, \quad (1)$$

is then produced. At $\vec{p} = \vec{0}$ a definite parity can be projected out using the operator

$$\Gamma_{\pm} = \frac{1}{2}(\gamma_0 \pm I). \quad (2)$$

Defining $G_{ij}(\vec{p}, t) = \text{Tr}(\Gamma \mathcal{G}_{ij}(\vec{p}, t))$, we can write the Dirac-traced correlation function as a sum of exponentials,

$$G_{ij}(t) = \sum_{\alpha} \lambda_i^{\alpha} \bar{\lambda}_j^{\alpha} e^{-m_{\alpha} t}. \quad (3)$$

Here λ_i^{α} and $\bar{\lambda}_j^{\alpha}$ are the couplings of the annihilation, χ_i, and creation, $\bar{\chi}_j$, operators at the sink and source respectively, while the energy eigenstates of mass m_{α} are enumerated by α. We then search for a linear combination of operators

$$\bar{\phi}^{\alpha} = \bar{\chi}_j u_j^{\alpha} \quad \text{and} \quad \phi^{\alpha} = \chi_i v_i^{\alpha} \quad (4)$$

such that ϕ and $\bar{\phi}$ couple to a single energy eigenstate. It is then clear from Eq. (3) that

$$G_{ij}(t_0 + dt) u_j^{\alpha} = e^{-m_{\alpha} dt} G_{ij}(t_0) u_j^{\alpha}, \quad (5)$$

and therefore for a given choice of variational parameters (t_0, dt), u_j^{α} and v_i^{α} can be obtained by solving the left and right eigenvalue equations

$$[G^{-1}(t_0) G(t_0 + dt)]_{ij} u_j^{\alpha} = c^{\alpha} u_i^{\alpha} \quad (6)$$

$$v_i^{\alpha} [G(t_0 + dt) G^{-1}(t_0)]_{ij} = c^{\alpha} v_j^{\alpha}, \quad (7)$$

with eigenvalue $c^{\alpha} = e^{-m_{\alpha} dt}$. We note that G_{ij} is a symmetric matrix in the ensemble average and as such we work with the improved estimator $\frac{1}{2}(G_{ij} + G_{ji})$ that ensures the eigenvalues of Eqs. (6) and (7) are equal. At t_0 and $t_0 + dt$ the eigenvectors u_j^{α} and v_i^{α} diagonalize the correlation matrix which enables us to write down the eigenstate-projected correlation function as

$$G^{\alpha}(t) = v_i^{\alpha} G_{ij}(t) u_j^{\alpha}. \quad (8)$$

$G^{\alpha}(t)$ is then used to extract masses. The energy spectrum of the lattice eigenstates is performed by fitting a single state ansatz to the eigenstate-projected correlator $G^{\alpha}(t)$, using a covariance matrix based χ^2 analysis as detailed in

Ref. [21]. At this point it is worth noting the key points that differentiate our projected correlator analysis from studies that make fits to the principal correlator.

The principal value of the correlator (for the state α) is defined as $c^{\alpha}(t, t_0)$, where the eigenvalue c^{α} as a function of time t is obtained by fixing an initial time t_0, then repeatedly solving the generalized eigenvalue problem (GEVP), as in Eq. (6), for increasing values of $t = t_0 + dt$. In the large time limit, $c^{\alpha}(t, t_0)$ will be proportional to the exponential of the energy of the state, $e^{-m_{\alpha}(t-t_0)}$. However, in practice, there is only a limited time window over which the GEVP can be solved before the problem breaks down due to loss of signal. At early times the value of $c^{\alpha}(t, t_0)$ is strongly influenced by excited state contamination [27], so studies using the principal value of the correlator typically use a two-exponential fit to extract the relevant energy level [2]. As a consequence of this, a two-exponential fit to the principal correlator provides enough parameter freedom such that the energy levels extracted may not be robust under a change of operator basis, and it is possible for missing states to influence the energy levels obtained from fits to $c^{\alpha}(t, t_0)$ [28,29].

Early CSSM studies of the variational method [27,30] found that the eigenvector components which define the optimized linear combination of operators for a particular state show only a weak dependence on the variational parameters (t, t_0). Hence, the variational analysis is ideally performed at early times where the excited states are contributing substantially to the correlation matrix and the uncertainties in the correlators are small, before loss of signal for the higher energy states spoils the convergence of the full GEVP. This need contrasts the desire to fit at large t where only a single state is contributing to a given correlator.

The eigenstate-projected correlator method bridges these two otherwise incompatible needs. We choose the variational parameters within the ideal region to solve the GEVP once and obtain a single set of optimized operators, such that the large time behavior of the projected correlator $G^{\alpha}(t)$ is well determined, as (unlike the principal correlator) it does not depend on the convergence of the GEVP at late times. Using the reduced χ^2 as a guide, we can search for an appropriate fit window in which the single-state ansatz is supported by $G^{\alpha}(t)$ and extract the lattice energy level for that state. Our most comprehensive analysis of the sensitivity of the excited state spectrum on missing states demonstrates that using the eigenstate-projected correlator method, one can extract robust energy levels, even when lower-lying states are missing [21].

III. INTERPOLATING FIELDS

We now turn our attention toward the selection of interpolating operators. As discussed in Sec. I, previous work with five-quark operators [15,21] have successfully extracted states consistent with scattering thresholds in the negative-parity nucleon channel. Of particular note is Ref. [15] in which a state consistent with the S-wave πN scattering threshold was extracted with a high degree of precision after explicitly projecting single-hadron momentum onto each single-hadron factor of the five-quark operator. Both of these calculations employed a πN-type negative-parity five-quark operator, constructed with a negative-parity meson piece and a positive-parity nucleon piece. Motivated by this success, we investigate a similar tactic in the positive-parity channel. Here, we construct five-quark operators with a positive-parity meson piece and a positive-parity nucleon piece.

Utilizing the operators for the positive-parity isoscalar σ and isovector a_0^0 and a_0^+ mesons

$$\sigma = \frac{1}{\sqrt{2}}[\bar{u}^e I u^e + \bar{d}^e I d^e],$$

$$a_0^0 = \frac{1}{\sqrt{2}}[\bar{u}^e I u^e - \bar{d}^e I d^e],$$

$$a_0^+ = [\bar{d}^e I u^e], \qquad (9)$$

we can construct five-quark σN- and $a_0 N$-type interpolators. Note that the labels $(\pi N, \sigma N, a_0 N)$ applied to our five-quark interpolators are solely meant to distinguish the mathematical structure, as each of these operators will excite multiple different states on the lattice. Recalling that the σ meson has the same quantum numbers as the vacuum we are able to write down the general form of the σN-type interpolators as

$$\chi_{\sigma N}(x) = \frac{1}{2} \epsilon^{abc}[u^{Ta}(x)\Gamma_1 d^b(x)]\Gamma_2 u^c(x)$$
$$\times [\bar{u}^e(x) I u^e(x) + \bar{d}^e(x) I d^e(x)]. \qquad (10)$$

Here, the choices of $(\Gamma_1, \Gamma_2) = (C\gamma_5, I)$ and (C, γ_5) provide us with two five-quark operators $\chi_{\sigma N}(x)$ and $\chi'_{\sigma N}(x)$ respectively.

Similarly, we write down the general form of the $a_0 N$-type operators using the Clebsch-Gordan coefficients to project isospin $I = 1/2$, $I_3 = +1/2$ obtaining

$$\chi_{a_0 N}(x) = \frac{1}{\sqrt{6}} \epsilon^{abc}$$
$$\times \{ 2[u^{Ta}(x)\Gamma_1 d^b(x)]\Gamma_2 d^c(x)[\bar{d}^e(x) I u^e(x)]$$
$$- [u^{Ta}(x)\Gamma_1 d^b(x)]\Gamma_2 u^c(x)[\bar{d}^e(x) I d^e(x)]$$
$$+ [u^{Ta}(x)\Gamma_1 d^b(x)]\Gamma_2 u^c(x)[\bar{u}(x)^e I u^e(x)]\}, \qquad (11)$$

where the two aforementioned choices of (Γ_1, Γ_2) provide $\chi_{a_0 N}(x)$ and $\chi'_{a_0 N}(x)$ respectively. In addition, we include the two five-quark operators $\chi_{\pi N}$ and $\chi'_{\pi N}$ based on the form

$$\chi_{\pi N}(x) = \frac{1}{\sqrt{6}} \epsilon^{abc} \gamma_5$$
$$\times \{2[u^{Ta}(x)\Gamma_1 d^b(x)]\Gamma_2 d^c(x)[\bar{d}^e(x)\gamma_5 u^e(x)]$$
$$- [u^{Ta}(x)\Gamma_1 d^b(x)]\Gamma_2 u^c(x)[\bar{d}^e(x)\gamma_5 d^e(x)]$$
$$+ [u^{Ta}(x)\Gamma_1 d^b(x)]\Gamma_2 u^c(x)[\bar{u}(x)^e\gamma_5 u^e(x)]\}, \quad (12)$$

and detailed in Ref. [21]. Our basis of qualitatively different operators is completed with the inclusion of the standard three-quark nucleon operators χ_1 and χ_2 given by

$$\chi_1 = \epsilon^{abc}[u^{aT}(C\gamma_5)d^b]u^c$$
$$\chi_2 = \epsilon^{abc}[u^{aT}(C)d^b]\gamma_5 u^c. \quad (13)$$

With the introduction of five-quark operators having an antiquark flavor matching one of the quark flavors, diagrams that contain loop propagators $S(y, y)$ where the source and sink position coincide are encountered. Loops at the source, $S(0, 0)$, can be treated with conventional propagators via $S(x, 0)|_{x=0}$. Loops at the sink, $S(x, x)$, are stochastically estimated by averaging over four independent $\mathbb{Z}_4$ noise vectors that are fully diluted in time, spin and color. Further details of our calculation of these stochastic propagators, along with the method by which they are smeared, can be found in our previous work [21].

IV. SIMULATION DETAILS

The results presented herein utilize the PACS-CS $2 + 1$ flavor dynamical-fermion configurations [31] with an Iwasaki gauge action [32] which are made available through the International Lattice Data Grid (ILDG) [33]. The lattice size is $32^3 \times 64$ with a lattice spacing of 0.0907 fm which provides a physical volume of $\approx (2.90 \text{ fm})^3$. The light quark mass is set by the hopping parameter $\kappa_{ud} = 0.13754$ which gives a pion mass of $m_\pi = 411$ MeV, while the strange quark mass is set by $\kappa_s = 0.13640$. Backward propagating states are removed via the imposition of fixed boundary conditions in the time direction [27,34].

The source insertion occurs at time slice $t_{\text{src}} = n_t/4 = 16$, well away from the boundary and its associated effects. Our variational analysis is performed with parameters $(t_0, dt) = (17, 3)$ which provides a good balance between systematic and statistical uncertainties. Error bars are calculated via single elimination jackknife, while a full covariance matrix analysis provides the χ^2/dof, which is used to select appropriate fit regions for eigenstate-projected correlators.

Gauge-invariant Gaussian smearing [35] at the source and sink is used to increase the span of our basis by altering the overlap of our interpolators with the states of interest. We investigate three levels of $n_s = 35, 100$ and 200 sweeps of Gaussian smearing.

V. RESULTS

A. Correlation matrix construction

As we now possess eight qualitatively different operators, each with three different levels of Gaussian smearing, our basis of twenty-four operators admits a substantial number of possible sub-bases of interest. Consequently, it is instructive to investigate various ratios of correlators, in order to determine which combinations can provide suitable sub-bases such that the condition number of the correlation matrix is favorable.

In Fig. 1 we present plots at each of the three smearing levels studied, showing a ratio of correlators formed by dividing each correlator with the correlation function formed from the standard χ_1 operator. Our aim is to identify correlators showing a unique approach to the plateau, indicating a novel superposition of excited states.

Notably, the ratios formed from the σN type operators, that is $G_{\chi_{\sigma N}}/G_{\chi_1}$ and $G_{\chi'_{\sigma N}}/G_{\chi_1}$ behave in a remarkably similar manner to the ratios G_{χ_1}/G_{χ_1} and G_{χ_2}/G_{χ_1}. Consequently, we anticipate the overlap of $\chi_{\sigma N}$ with states in the spectrum is very similar to χ_1 and similarly the overlap of states with $\chi'_{\sigma N}$ is much the same as with χ_2. Evidently, these new σN-type operators provide little new information from that already contained in χ_1 and χ_2. Recalling that the σ meson carries the quantum numbers of the vacuum provides some insight into this result. In light of this similarity, the $\chi_{\sigma N}$ and $\chi'_{\sigma N}$ interpolators are omitted from bases that also contain the matching χ_1 or χ_2 interpolator.

Of the two new $a_0 N$ interpolators, $\chi_{a_0 N}$ stands out from the other interpolators at all three smearing levels. $\chi_{a_0 N}$ excites a novel superposition of nucleon excited states and will aid in spanning the space of low-lying states. It holds promise to reveal the presence of a low-lying state missed in previous analyses. Similarly, at 100 and especially 200 smearing sweeps, $\chi'_{a_0 N}$ shows a unique path to the plateau, again indicating the promise of disclosing new states.

In comparing the various smearing levels for all the correlator ratios presented, one observes that the plateau in the ratios occurs at earlier times as the smearing increases. Again, these differences between different smearing levels aid in spanning the space and generating correlation matrices with good condition numbers. However, the construction of large correlation matrices tends to increase the condition number and decrease the likelihood of obtaining a solution. This effect, combined with the larger statistical uncertainties encountered with the largest smearing extent, leads to difficulties in finding a solution to the generalized eigenvalue equations with the new five-quark operators.

As a result, we focus on correlation matrices formed from 35 and 100 sweeps of smearing in the propagator sources and sinks. These are the smearing levels that provide the most variation at early times, and hence the
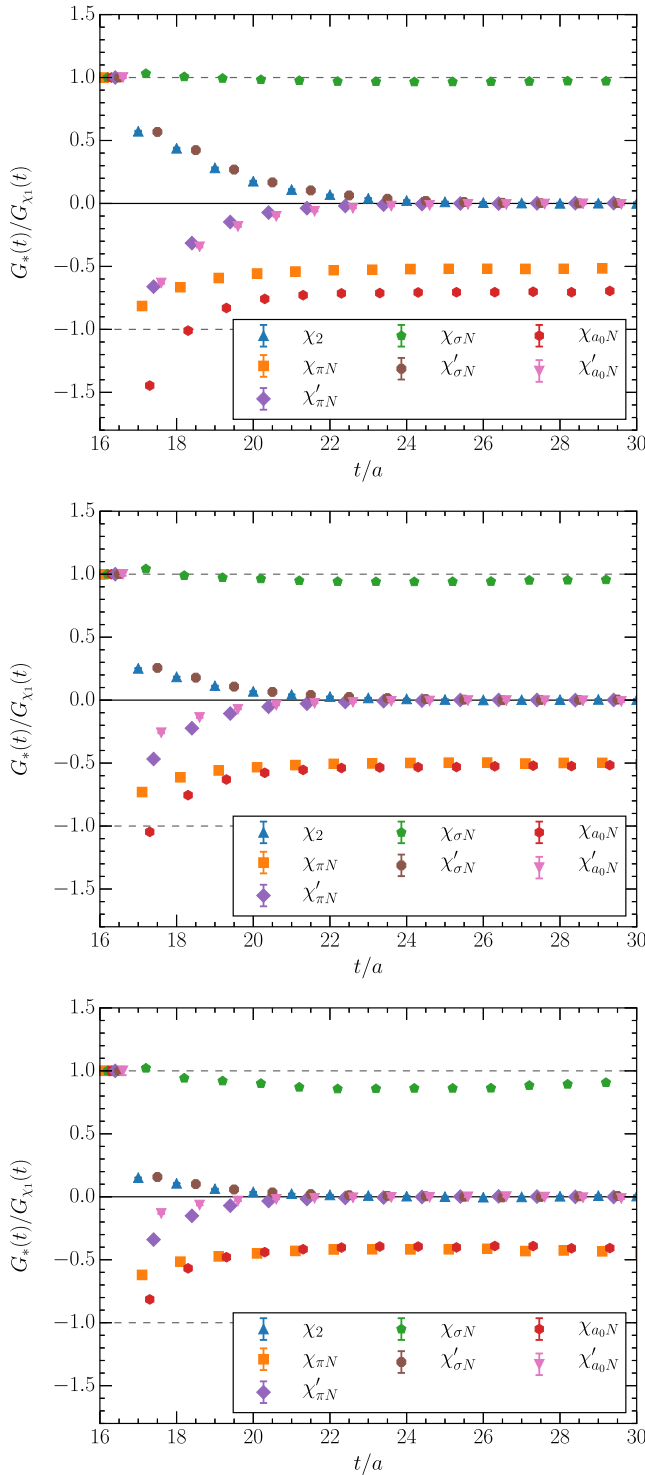
FIG. 1. Correlation function ratios constructed to illustrate different superpositions of energy eigenstates in the correlators. The ratio is formed by dividing the correlator corresponding to each operator indicated in the legend by the correlation function formed from the χ_1 operator. Plots are presented at 35 (top), 100 (middle) and 200 (bottom) sweeps of Gaussian smearing in the quark-propagator source and sink. For clarity of presentation, the t component of the ratio is sequentially offset.

levels at which we are able to construct bases more likely to provide an effective span of the state space, particularly in comparison to that obtained using three-quark operators alone. This enables us to examine scenarios with multiple, qualitatively different quark structures, while still retaining the presence of multiple smearing levels. While we will not detail the results including the 200 sweep correlators, we do note that when a solution was found, the energies of the low-lying eigenstates agreed with the results presented in the following.

We consider seven different correlation matrices formed from the bases outlined in Table I. Each basis is formed with 35 and 100 sweeps of smearing, thus creating four 8×8 bases, two 6×6 bases and one 4×4 basis. While each correlation matrix may disclose different states, the energies of the states observed should agree among the different bases considered.

B. Finite volume spectrum of states

The development of Hamiltonian effective field theory [22,23,36] can provide some insight into the spectrum to be anticipated. By using an effective field theory model constrained to the experimental phase shifts, inelasticities and pole position, one can predict the spectrum to be observed in the finite volume of the lattice. In Ref. [22], three models are considered with different roles played by the bare basis-state in constructing the Hamiltonian model. In the popular model incorporating a bare basis state with a mass of 2.0 GeV, the model predicts a Roper-like state at 1750 MeV in the finite volume of the lattice for the quark mass corresponding to $\kappa = 0.13754$ that is considered herein.

Alternatively, the third model of Ref. [22], preferred by previous lattice results, predicts the absence of low-lying states with a strong bare-state component, predicting instead the existence of five meson-baryon scattering states below the state observed in lattice QCD, commencing at 1600 MeV. Attraction in these channels could localize the meson to the vicinity of the baryon [37], overcoming the volume suppression of the coupling.

The low-lying spectra produced from the correlation matrices detailed in Table I are presented in Fig. 2. In basis

TABLE I. The interpolating fields used in constructing each correlation-matrix basis.

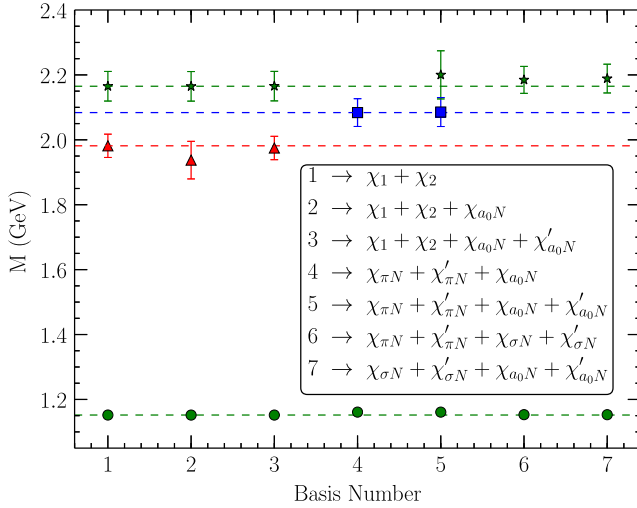| Basis Number	Operators Used
1	χ_1, χ_2
2	$\chi_1, \chi_2, \chi_{a_0N}$
3	$\chi_1, \chi_2, \chi_{a_0N}, \chi'_{a_0N}$
4	$\chi_{\pi N}, \chi'_{\pi N}, \chi_{a_0N}$
5	$\chi_{\pi N}, \chi'_{\pi N}, \chi_{a_0N}, \chi'_{a_0N}$
6	$\chi_{\pi N}, \chi'_{\pi N}, \chi_{\sigma N}, \chi'_{\sigma N}$
7	$\chi_{\sigma N}, \chi'_{\sigma N}, \chi_{a_0N}, \chi'_{a_0N}$

FIG. 2. Low-lying states observed for each of the correlation-matrix bases described in Table I. For each interpolating field, two smearing levels of $n_s = 35$ and $n_s = 100$ are used in all cases. Dashed horizontal lines are present to guide the eye. They have been set by the central values from basis 1 in all cases except for the state ~ 2.1 GeV, in which case it is drawn from basis 4.

number one, we present results from a simple 4×4 analysis with the three-quark χ_1 and χ_2 interpolating fields at two different smearing levels. This consideration of three-quark operators alone [1,12] provides the benchmark analysis that we will refer to as we attempt to ascertain whether subsequent bases with five-quark operators alter the low-lying spectrum.

As previously mentioned, χ_{a_0N} appeared to be the most promising new operator, in that the ratio χ_{a_0N}/χ_1 displayed the largest variation when compared to ratios previously studied. As such, in column two we add the χ_{a_0N} operator to χ_1 and χ_2 and perform the resulting 6×6 correlation matrix analysis. This analysis reveals no new low-lying states. We then further add the χ'_{a_0N} operator forming an 8×8 analysis. Once again the spectrum is invariant, revealing no new states.

As the overlap of three-quark operators with three-quark states is naturally large when compared to five-quark operators, we proceed by considering bases that contain only five-quark operators. The aim is to allow spectral strength that may have ordinarily been overwhelmed by three-quark operators to come to the fore. Such an approach was beneficial in the odd-parity nucleon sector [21].

The results of a 6×6 analysis using $\chi_{\pi N}$, $\chi'_{\pi N}$ and χ_{a_0N} are illustrated as basis number four in Fig. 2. Here, we observe an energy level that lies between the two previously observed states, but crucially no new low-lying state is extracted. In the final three columns we form 8×8 bases with the three possible combinations of pairs of our five-quark operators. States consistent with those already observed are extracted, including the excited energy level in basis four, but once again no new low-lying states are found.

Returning to the aforementioned Hamiltonian effective field theory model [22], there are some common features in the spectrum. The splitting of ~ 200 MeV between the first and second excitations observed with the three-quark operators is similar to that predicted by the model. More interesting is the model's prediction of a scattering state with a dominant πN component roughly half way between the two excitations. In bases four and five, containing $\chi_{\pi N}$ and $\chi'_{\pi N}$ interpolators, we do observe an energy level roughly half way between the two excitations. The dismissal of three-quark operators is key to the appearance of this level. However, the lattice data is insufficient to definitively conclude that this energy level is a new state, as none of the bases studied yield three orthogonal excited states simultaneously.

While these qualitative features are consistent, the goal of this investigation was to reveal new states below the lowest-lying excitation of three quark operators through the consideration of novel five-quark operators. We are now able to conclude that the introduction of positive-parity mesons in local five-quark operators of the nucleon, does not provide strong overlap with the anticipated low-lying finite-volume scattering states.

However, these operators do have strong overlap with the ground state nucleon, once again highlighting the meson-baryon cloud of the nucleon. In bases four through seven, only five-quark operators are considered and we are able to extract the ground state mass with a high degree of precision, comparable to that obtained solely with three-quark operators.

VI. CONCLUSIONS

In this exploratory investigation we have introduced local five-quark operators with the quantum numbers of the Roper resonance, based on combining positive-parity mesons with conventional nucleon interpolators. Drawing on success in the negative parity channel, the aim was to reveal new low-lying states that had been missed in previous calculations utilizing three-quark operators. The construction of a_0N- and σN-type interpolating fields was outlined and variational analyses were performed with these new interpolating fields, in combination with previously considered πN-type and standard three-quark interpolators.

Ratios of correlation functions were examined to discover which interpolators gave rise to new superpositions of excited states and therefore which interpolators held the greatest promise of overlapping with new states. This process indicated that the χ_{a_0N} operator was the most promising interpolator for revealing new low-lying states.

Correlation matrices were constructed from several different bases of interpolating operators. By systematically varying the operators used, the independence of the low-lying spectrum from the basis could be checked and the

potential for new state discovery was increased. In accord with previous studies, changing the operators composing the basis of a correlation matrix does affect whether or not a particular state is observed.

No new states below the first excitation found with three-quark operators were observed. The local five-quark operators studied were found to posses a strong overlap with the ground state nucleon, as bases containing only these operators produced a ground state with a high degree of precision.

Comparing to the predictions of the Hamiltonian effective field theory study mentioned earlier [22], we do not find a lattice energy level near 1750 MeV as predicted by Scenario I (which postulates a localized Roper bare state). The fact that this state has not been observed herein indicates that Scenario III is preferred, which predicts a localized lattice energy level near 2.0 GeV at this pion mass, consistent with our results.

We conclude that the low-lying finite-volume meson-baryon scattering states anticipated by Hamiltonian effective field theory are not well localized. Instead, the two-particle scattering component appears to dominate such that the volume suppression of these scattering states with local operators prevents their strong overlap with the interpolators considered herein. The fact that we do not find any low-lying localized states casts doubt on molecular models of the Roper. Our results strengthen the interpretation of the Roper as a coupled-channel dynamically-generated meson-baryon resonance, a resonance not closely associated with conventional three-quark states.

[1] M. S. Mahbub, W. Kamleh, D. B. Leinweber, P. J. Moran, and A. G. Williams, Phys. Lett. B **707**, 389 (2012).

[2] R. G. Edwards, J. J. Dudek, D. G. Richards, and S. J. Wallace, Phys. Rev. D **84**, 074508 (2011).

[3] C. D. Roberts, I. C. Cloet, L. Chang, and H. L. Roberts, AIP Conf. Proc. **1432**, 309 (2012).

[4] T. Bauer, J. Gegelia, and S. Scherer, Phys. Lett. B **715**, 234 (2012).

[5] D. S. Roberts, W. Kamleh, and D. B. Leinweber, Phys. Lett. B **725**, 164 (2013).

[6] K.-F. Liu, Y. Chen, M. Gong, R. Sufian, M. Sun *et al.*, *Proc. Sci.*, LATTICE2013 (2014) 507, [arXiv:1403.6847].

[7] N. Isgur and G. Karl, Phys. Lett. B **72B**, 109 (1977).

[8] N. Isgur and G. Karl, Phys. Rev. D **19**, 2653 (1979).

[9] L. Y. Glozman and D. Riska, Phys. Rep. **268**, 263 (1996).

[10] J. Speth, O. Krehl, S. Krewald, and C. Hanhart, Nucl. Phys. **A680**, 328 (2000).

[11] T. Burch, C. Gattringer, L. Y. Glozman, R. Kleindl, C. B. Lang, and A. Schaefer (Bern-Graz-Regensburg), Phys. Rev. D **70**, 054502 (2004).

[12] M. S. Mahbub, A. O. Cais, W. Kamleh, B. G. Lasscock, D. B. Leinweber, and A. G. Williams, Phys. Lett. B **679**, 418 (2009).

[13] D. S. Roberts, W. Kamleh, and D. B. Leinweber, Phys. Rev. D **89**, 074501 (2014).

[14] P. C. Bruns, M. Mai, and U. G. Meissner, Phys. Lett. B **697**, 254 (2011).

[15] C. B. Lang and V. Verduci, Phys. Rev. D **87**, 054502 (2013).

[16] M. S. Mahbub, W. Kamleh, D. B. Leinweber, P. J. Moran, and A. G. Williams, Phys. Rev. D **87**, 011501 (2013).

[17] M. S. Mahbub, W. Kamleh, D. B. Leinweber, and A. G. Williams, Ann. Phys. (Berlin) **342**, 270 (2014).

[18] M. S. Mahbub, W. Kamleh, D. B. Leinweber, P. J. Moran, and A. G. Williams, Phys. Rev. D **87**, 094506 (2013).

[19] R. G. Edwards, N. Mathur, D. G. Richards, and S. J. Wallace (Hadron Spectrum), Phys. Rev. D **87**, 054506 (2013).

[20] J. Bulava, R. G. Edwards, E. Engelson, B. Joo, H.-W. Lin, C. Morningstar, D. G. Richards, and S. J. Wallace, Phys. Rev. D **82**, 014507 (2010).

[21] A. L. Kiratidis, W. Kamleh, D. B. Leinweber, and B. J. Owen, Phys. Rev. D **91**, 094509 (2015).

[22] Z.-W. Liu, W. Kamleh, D. B. Leinweber, F. M. Stokes, A. W. Thomas, and J.-J. Wu, Phys. Rev. D **95**, 034034 (2017).

[23] J. M. M. Hall, W. Kamleh, D. B. Leinweber, B. J. Menadue, B. J. Owen, A. W. Thomas, and R. D. Young, Phys. Rev. Lett. **114**, 132002 (2015).

[24] C. Michael, Nucl. Phys. **B259**, 58 (1985).

[25] M. Luscher and U. Wolff, Nucl. Phys. **B339**, 222 (1990).

[26] D. Leinweber, W. Kamleh, A. Kiratidis, Z.-W. Liu, S. Mahbub, D. Roberts, F. Stokes, A. W. Thomas, and J. Wu, J. Phys. Soc. Jpn. Conf. Proc. **10**, 010011 (2016).

[27] M. S. Mahbub, A. Ó. Cais, W. Kamleh, B. G. Lasscock, D. B. Leinweber, and A. G. Williams, Phys. Rev. D **80**, 054507 (2009).

[28] J. J. Dudek, R. G. Edwards, and C. E. Thomas (Hadron Spectrum), Phys. Rev. D **87**, 034505 (2013); **90**, 099902(E) (2014).

[29] D. J. Wilson, R. A. Briceno, J. J. Dudek, R. G. Edwards, and C. E. Thomas, Phys. Rev. D **92**, 094502 (2015).

[30] M. S. Mahbub, W. Kamleh, D. B. Leinweber, A. O Cais, and A. G. Williams, Phys. Lett. B **693**, 351 (2010).

[31] S. Aoki, K. I. Ishikawa, N. Ishizuka, T. Izubuchi, D. Kadoh, K. Kanaya, Y. Kuramashi, Y. Namekawa, M. Okawa, Y. Taniguchi, A. Ukawa, N. Ukita, and T. Yoshie (PACS-CS Collaboration), Phys. Rev. D **79**, 034503 (2009).

[32] Y. Iwasaki, Report number UTHEP-118 (2011).

[33] M. G. Beckett, P. Coddington, B. Joó, C. M. Maynard, D. Pleiter, O. Tatebe, and T. Yoshie, Comput. Phys. Commun. **182**, 1208 (2011).

[34] W. Melnitchouk, S. Bilson-Thompson, F. D. R. Bonnet, J. N. Hedditch, F. X. Lee, D. B. Leinweber, A. G. Williams, J. M. Zanotti, and J. B. Zhang, Phys. Rev. D **67**, 114506 (2003).

[35] S. Gusken, Nucl. Phys. B, Proc. Suppl. **17**, 361 (1990).

[36] J. M. M. Hall, A. C.-P. Hsu, D. B. Leinweber, A. W. Thomas, and R. D. Young, Phys. Rev. D **87**, 094510 (2013).

[37] Z.-W. Liu, J. M. M. Hall, D. B. Leinweber, A. W. Thomas, and J.-J. Wu, Phys. Rev. D **95**, 014506 (2017).